

# Understanding Anharmonic Effects on Hydrogen Desorption Characteristics of $\text{Mg}_n\text{H}_{2n}$ Nanoclusters by ab initio trained Deep Neural Network

Andrea Pedrielli,<sup>†,‡</sup> Paolo E. Trevisanutto,<sup>¶</sup> Lorenzo Monacelli,<sup>§</sup> Giovanni  
Garberoglio,<sup>†,||</sup> Nicola M. Pugno,<sup>‡,⊥</sup> and Simone Taioli<sup>\*,†,||,#</sup>

<sup>†</sup>*European Centre for Theoretical Studies in Nuclear Physics and Related Areas  
(ECT\*-Fondazione Bruno Kessler)*

<sup>‡</sup>*Laboratory of Bioinspired, Bionic, Nano, Meta Materials & Mechanics, Department of  
Civil, Environmental and Mechanical Engineering, University of Trento, Italy*

<sup>¶</sup>*Faculty of Engineering Università Campus Bio-Medico, Rome, Italy*

<sup>§</sup>*Department of Physics, University of Rome La Sapienza, Rome, Italy*

<sup>||</sup>*Trento Institute for Fundamental Physics and Applications (TIFPA-INFN), Trento, Italy*

<sup>⊥</sup>*School of Engineering and Materials Science, Queen Mary University of London, UK*

<sup>#</sup>*Peter the Great St. Petersburg Polytechnic University, St. Petersburg, Russia*

E-mail: taioli@ectstar.eu

## Abstract

Magnesium hydride ( $\text{MgH}_2$ ) has been widely studied for effective hydrogen storage. However, its bulk desorption temperature (553 K) is deemed too high for practical applications. Besides doping, a strategy to decrease such reaction energy for releasing

hydrogen is the use of  $\text{MgH}_2$ -based nanoparticles (NPs). Here, we investigate first the thermodynamic properties of  $\text{Mg}_n\text{H}_{2n}$  NPs ( $n < 10$ ) from first-principles, in particular by assessing the anharmonic effects on the enthalpy, entropy and thermal expansion by means of the Stochastic Self Consistent Harmonic Approximation (SSCHA). The latter method goes beyond previous approaches, typically based on molecular mechanics and the quasi-harmonic approximation, allowing the ab initio calculation of the fully-anharmonic free energy. We find an almost linear dependence on temperature of the interatomic bond lengths – with a relative variation of few percent over 300 K –, alongside with a bond distance decrease of the Mg–H bonds. In order to increase the size of NPs toward experiments of hydrogen desorption from  $\text{MgH}_2$  we devise a computationally effective Machine Learning model trained to accurately determine the forces and total energies (i.e. the potential energy surfaces), integrating the latter with the SSCHA model to fully include the anharmonic effects. We find a significative decrease of the H-desorption temperature for sub-nanometric clusters  $\text{Mg}_n\text{H}_{2n}$  with  $n \leq 10$ , with a non-negligible, although little effect due to anharmonicities (up to 10%).

## Introduction

Hydrogen represents a low environmental impact energy vector provided that effective storage media can be found<sup>1–14</sup>. Among the most promising materials, bulk magnesium hydride ( $\text{MgH}_2$ ) presents considerable gravimetric hydrogen storage capacity (7.6 – 7.7 wt%<sup>15–18</sup>), being also abundant and relatively cheap. However, the 1 bar desorption temperature  $T_d$ , which is approximately 553 K (280°C) as well as the relatively slow absorption/desorption reaction kinetics hinder its possible use in real-life devices<sup>9</sup>. Nonetheless,  $T_d$  can be modified by pursuing several different routes, such as doping<sup>7,19</sup> and/or nanosizing of the storage materials<sup>4,20–22</sup>. In particular, the decreasing effect on  $T_d$  of nanosizing has been recently investigated by both experiments<sup>20–22</sup>, numerical simulations<sup>2–4,8,23–27</sup>, and analytical models<sup>28</sup>.

In this respect, a few computational studies focused on nanoparticles (NPs) that are trimmed from the crystalline bulk, finding a structural destabilization upon decreasing the volume-to-surface ratio. The destabilization of  $\text{MgH}_2$  NPs can be practically obtained through the synthesis of a metastable phase<sup>6,29,30</sup> – called  $\gamma\text{-MgH}_2$  – via ball-milling. However, at odds with this finding, recent computational results indicated that the non-crystalline geometries actually increase their stability<sup>2,4</sup> except for NPs containing only a few atoms. To carry out numerical simulations of the thermodynamic properties, in particular in  $\text{MgH}_2$  NPs, a variety of theoretical and computational methods have been used, such as Diffusion Monte Carlo (DMC), Coupled Cluster CCSD(T)<sup>2,25</sup>, and Density Functional Theory (DFT)<sup>4</sup>. We notice that while DMC and CCSD(T) are the most accurate methods, the general trend of the 0 K desorption energy can be also captured by DFT<sup>4</sup>. For example, DFT total energy calculations on small  $\text{MgH}_2$  NPs (validated by high-accuracy CCSD(T) simulations) devised a possible explanation for their destabilization<sup>25</sup>, by showing that while the desorption energy of hydrogen from crystalline samples approaches the bulk value with increasing size, the extrapolated desorption energy from amorphous NPs tends to a lower value (54 kJ/mol) which suits hydrogen storage applications. Furthermore, the 0 K desorption energies have been assessed by means of hybrid functional DFT calculations finding a good matching with DMC and CCSD(T) calculations<sup>4,25</sup>.

We stress that the whole of these ab initio studies are focused on reckoning the properties of  $\text{MgH}_2$  NPs at zero temperature, thus neglecting the effect of anharmonicity on entropy and enthalpy, and its possible impact on  $T_d$ . However, particularly in the case of small diameter NPs containing hydrogen, such effect can be significant<sup>31</sup>, and thus must be accounted for. In this respect, the anharmonic free energy is typically assessed either at classical level using force fields or from first-principles simulations within the harmonic or quasi-harmonic approximation<sup>31</sup>. For example, DFT calculations within the harmonic approximation to assess the thermodynamic properties of bulk  $\text{MgH}_2$  were reported<sup>3</sup>. However, within such approximation the reduction of the reaction enthalpy observed at experimental level by

decreasing the NPs size cannot be reproduced<sup>22</sup>. It is clear then that a proper assessment of the thermodynamic properties of  $\text{Mg}_n\text{H}_{2n}$  NPs should account for the accurate treatment of the anharmonicity.

In this work, we use first-principles simulations to determine the characteristic functions of state, such entropy and enthalpy, and the Gibbs free energy of Mg and  $\text{Mg}_n\text{H}_{2n}$  NPs fully including the anharmonicity by using the Stochastic Self Consistent Harmonic Approximation (SSCHA). SSCHA includes both anharmonicity and zero-point energy in the calculation of the free energy at an efficient computational cost reduction with respect to third and fourth-order perturbative approaches<sup>31–33</sup>. We also compute  $T_d$  for a number of  $\text{Mg}_n\text{H}_{2n}$  NPs, with  $n = 3 - 10$  at different levels of accuracy. In particular, we compared the harmonic approximation with the fully anharmonic approach given by the SSCHA method. Furthermore we introduced the rotational entropy contribution in the anharmonic case, which could be relevant in the case of unsupported NPs.

In this context, the possible enthalpy-entropy compensation has been proposed as the limiting mechanism preventing the decrease of  $T_d$ <sup>9,22</sup>.

We also present in the Supplementary Material a thorough investigation of the frontiers orbitals (HOMO–LUMO) for the  $\text{Mg}_n\text{H}_{2n}$  NPs computed at DFT-D3<sup>34</sup> level of theory.

Finally, to study realistic systems, such as those used in experiments, and derive possible trends of the thermodynamic observables with system size, we develop a Machine Learning (ML) model, which has been trained using our first-principles data to determine the forces and total energies (and then, the potential energy surfaces) of the  $\text{Mg}_n\text{H}_{2n}$  molecular clusters, with  $n \gg 10$ . In fact, the free energy calculation via the SSCHA method with DFT-evaluated energies limits the number of atoms of the NPs, and one needs to devise novel approaches that make a cheaper evaluation of the free energy and of the forces without sacrificing accuracy. Indeed, by using ML we carried out the calculations of thermodynamic properties at ab initio accuracy for  $\text{Mg}_n\text{H}_{2n}$  NPs up to  $n = 43$  on a laptop. To this purpose, we have employed the SchNet–package<sup>35</sup>, a continuous filter layers convolutional Neural-Network (NN) package

integrating the latter in the Atomic Simulation Environment (ASE)<sup>36</sup> together with the python implementation of the SSCHA code<sup>31-33</sup>.

This article is organized as follows. In section 2, we describe our methodological and computational approaches to the simulation of the thermodynamic properties with the inclusion of anharmonic effects. In this section we also discuss our ML model applied to the  $\text{Mg}_n\text{H}_{2n}$  NPs. In section 3, we use the SSCHA method for calculating the finite temperature properties of these  $\text{MgH}_2$  NPs and of their relevant  $T_d$  modified by the inclusion of anharmonicity. In section 4 we draw conclusions by summarizing our findings and discussing their applicability in further investigations.

## Theoretical and Computational Methods

### Thermodynamics of hydrogen desorption

The hydrogen desorption temperature  $T_d$  in  $\text{MgH}_2$  can be determined by reckoning the variation of the Gibbs free energy  $\Delta G = \Delta H - T\Delta S$  as function of the pressure, where  $\Delta H$  and  $\Delta S$  are the changes in enthalpy and entropy of the reaction at constant temperature and volume, respectively. Indeed, at constant pressure  $p = 1$  bar, the relation:

$$\ln\left(\frac{p}{p_0}\right) = -\frac{\Delta G}{RT_d} = 0, \tag{1}$$

where  $p_0 = 1$  bar and  $R$  is the universal gas constant, reads:

$$T_d = \frac{\Delta H(T)}{\Delta S(T)}. \tag{2}$$

Since in general both  $\Delta H$  and  $\Delta S$  are temperature-dependent functions,  $T_d$  is the value that fulfills the following implicit equation

$$f(T) = T - \frac{\Delta H(T)}{\Delta S(T)} = 0. \tag{3}$$

Enthalpy and entropy of both  $\text{Mg}_n\text{H}_{2n}$  NPs and molecular hydrogen can be computed from ab initio simulations of  $\Delta G$  at various temperatures. In particular,  $\text{H}_2$  simulations were performed by considering a ortho- to para-hydrogen ratio of 3 : 1.  $\Delta G$  is an outcome of SSCHA calculations. While the latter method is generally used for periodic structures<sup>31–33</sup>, recent developments have enlarged its scope to structures with a large number of degrees of freedom and finite systems, such as NPs or large molecules.

From the knowledge of  $\Delta G$ , we computed the entropy  $S$  at constant pressure (and of course, number of atoms) as:

$$S(T) = - \left. \frac{\partial G(T)}{\partial T} \right|_p, \quad (4)$$

while the enthalpy can be derived from:

$$H(T) = G(T) + TS(T). \quad (5)$$

## Stochastic Self Consistent Harmonic Approximation

The SSCHA method<sup>31–33,37</sup> is based on a variational approach and delivers an accurate description of the phonon bands in non-perturbative regime. The Helmholtz free energy (HFE) of a solid, which includes the contributions arising from the static lattice zero-temperature internal energy, from the thermal electronic excitation and from the ionic vibrations, reads<sup>38</sup>:

$$F_{\mathcal{H}} = \text{Tr}(\rho_{\mathcal{H}} \mathcal{H}) + \frac{1}{\beta} \text{Tr}(\rho_{\mathcal{H}} \ln \rho_{\mathcal{H}}) \quad (6)$$

where  $\mathcal{H} = K + V$  is the total Hamiltonian of the system written as the sum of kinetic energy operator ( $K$ ) and of the many-body adiabatic potential energy ( $V$ ) within the Born–Oppenheimer approximation. In Eq. 6  $\rho_{\mathcal{H}} = e^{-\beta \mathcal{H}} / [\text{Tr}(e^{-\beta \mathcal{H}})]$  is the density matrix, where  $\beta = 1/(k_{\text{B}}T)$ ,  $k_{\text{B}}$  is the Boltzmann constant, and  $T$  the temperature.

The Gibbs–Bogoliubov variational principle states that for an arbitrary trial Hamiltonian

$\mathcal{H} = K + \mathcal{V}$ , the HFE fulfills the following inequality:

$$F_{\mathcal{H}} \leq \mathcal{F}_{\mathcal{H}}[\mathcal{H}] = F_{\mathcal{H}} + \int d\mathbf{R} [V(\mathbf{R}) - \mathcal{V}(\mathbf{R})] \rho_{\mathcal{H}}(\mathbf{R}) \quad (7)$$

where  $\mathbf{R}$  identifies the ion positions. In the SSCHA method the minimization of  $\mathcal{F}_{\mathcal{H}}[\mathcal{H}]$  is performed by a stochastic evaluation of the free energy and its gradient by varying the free parameters of an Hamiltonian characterised by an harmonic trial potential  $\mathcal{V}$ . During the minimization, the atomic coordinates are allowed to relax in order to obtain the finite temperature atomic positions.

In this work, we assume that the vibrational, rotational, and translational degrees of freedom are completely separable, and further that the MgH<sub>2</sub> nanoclusters can be considered as rigid rotors. The atomic coordinates used for the rotational entropy calculation are however optimized at finite temperature within the SSCHA.

Thus, the translational and rotational degrees of freedom do not enter in the simulation of the SSCHA free energy, and they are considered zero-frequency modes. However, their contribution to the free energy can be assessed from statistical mechanics owing to the relatively high temperatures under investigation.

To obtain accurate free energies (within a few meV), we progressively increased the stochastic populations up to a few thousands configurations. The calculations have been performed at 300 K, 500 K, and 600 K. The free energy calculation has been extended in the range  $\pm 20$  K around each calculated point, using the stochastic population generated at the reference temperature by taking advantage of the reweighting procedure<sup>33</sup>. We used these data points and the associated stochastic error to derive by weighted interpolation the thermodynamic quantities as functions of temperature.

SSCHA proceeds through a series of repeated evaluation steps, the first being the generation of the stochastic population and the calculation of the energy and forces for each element of the population, the second being the minimization of the free energy using a

reweighting procedure. The resampling is performed when the stochastic population due to the reweighting procedure is no more representative of the starting one. Convergence studies are reported in the Supporting Information.

## **Ab initio calculation of the Born-Oppenheimer potential surfaces and forces**

The SSCHA relies on the minimization of the free energy of the variational harmonic system by stochastic evaluation of the  $N$ -dimensional potential surface. This method starts by an ansatz on the force-constant matrix, which is typically assumed to be the harmonic one. We performed the evaluation of the potential energy, forces and dynamical matrix by means of DFT calculations, using the QUANTUM ESPRESSO code suite<sup>39</sup>.

The ion-electron interaction was treated by the PBE exchange-correlation functional<sup>40</sup>. The van der Waals dispersion forces were included via the Grimme D3 semiempirical correction<sup>41</sup>. NPs properties were computed within a cubic cell of 2 nm side for all structures, which is sufficient to avoid periodic image spurious interactions. Furthermore, to cutoff interactions among periodic replicas we used the Makov–Payne<sup>42</sup> correction. With our simulation cell we obtained consistent results also using the Martyna–Tuckerman<sup>43</sup> correction.

To achieve fully converged energies and forces the kinetic energy cutoff of the plane wave basis set has been fixed to 80 Ry, while the charge density cutoff four times as high. The self-consistent threshold has been set to  $10^{-8}$  Ry. The  $k$ -points sampling consists of the  $\Gamma$ -point only, owing to the finite nature of the MgH<sub>2</sub> nanostructures.

## **Structure of Mg and MgH<sub>2</sub> nanoparticles**

To reckon  $T_d$  and the equilibrium thermodynamic properties is crucial to find the atomic arrangements of the MgH<sub>2</sub> NPs in a global free energy minimum. This task is prohibitively demanding owing to the large computational cost of determining from ab initio simulations



the lowest energy configurations of clusters with an increasing number of atomic centers.

To include the anharmonic effects in the geometry optimization of  $\text{Mg}_n\text{H}_{2n}$  NPs ( $n \leq 10$ ) we start from structures corresponding to local minima of the relevant potential energy surfaces<sup>4,26,27</sup>. These geometries are then fully relaxed at finite temperature using the SSCHA method. The optimized atomic positions are selected as the centroid of the stochastic population.

To start the structural optimization of  $\text{Mg}_n\text{H}_{2n}$  NPs ( $n \geq 10$ ), we used the geometries of  $\text{Ti}_n\text{O}_{2n}$  NPs ( $n = 15, 20, 43$ ) as by Ref.<sup>44</sup>, on the basis of their similarity (other geometries of  $\text{Ti}_n\text{O}_{2n}$  clusters potentially suitable can be found in Refs.<sup>45,46</sup>).

We report in Figs. 1 and 2 a sketch of the 300 K optimized  $\text{Mg}_n$  and  $\text{Mg}_n\text{H}_{2n}$  NPs ( $n \leq 10$ ), for which  $T_d$  has been calculated.

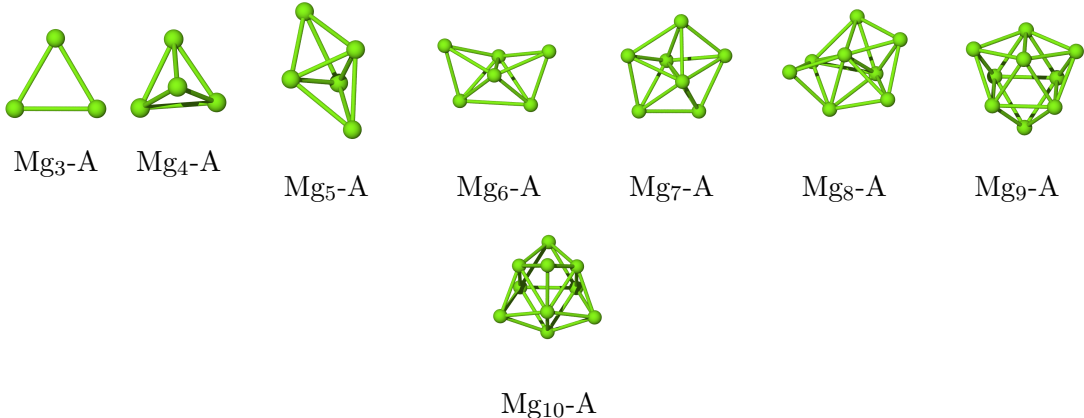


Figure 1: Optimized  $\text{Mg}_n$  nanostructures at 300 K with the inclusion of anharmonic corrections via SSCHA.

As non-stoichiometric NPs at 0 K are less stable than stoichiometric  $\text{Mg}_n\text{H}_{xn}$  clusters<sup>47</sup> (even though substoichiometric concentration for  $n > 6, x = 0.4$  are potentially interesting for hydrogen storage owing to their lower  $T_d$ <sup>25</sup>) we limit our focus to the latter ones.

### Machine Learning approach: the SchNet–SSCHA algorithm

To increase the size of  $\text{MgH}_2$  NPs beyond the dimension feasible via first-principles methods, a ML model has been trained to determine the forces and the total energies (i.e. the potential

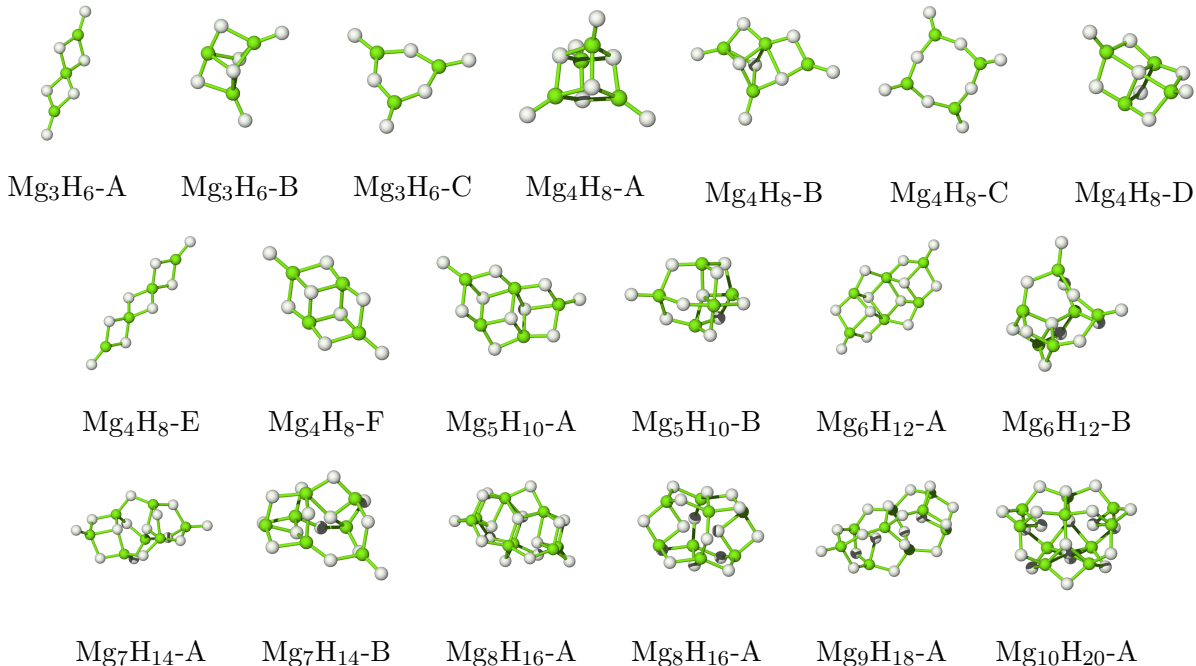


Figure 2: Optimized  $\text{MgH}_2$  nanostructures at 300 K with the inclusion of anharmonic corrections via SSCHA.

energy surfaces) of the molecular clusters. The NN training set for the SchNet-SSCHA (S[chnet]SCHA) calculations is limited to energy and forces corresponding to the SSCHA populations at 300 and 500 K, thus is not suitable for the description of the different phases that can be crossed in the minima mining. To this purpose, we have employed SchNet<sup>35</sup>, which is a continuous filter layers convolutional Neural-Network (NN) package.

We tested our S[chnet]SCHA approach for calculating the thermodynamic properties of  $\text{Mg}_n\text{H}_{2n}$  NPs ( $n \geq 10$ ). In this respect, the training set contains  $2 \times 10^5$   $\text{Mg}_n$  and  $\text{Mg}_n\text{H}_{2n}$  cluster configurations ( $3 \leq n \leq 10$ ) with their relevant DFT forces and total energies. The validation set contains  $4 \times 10^4$  configurations. Our NN is generated with 5 interaction blocks, 128 features and, for the Gaussian expansion, we used a range of  $25 \text{ \AA}$  to cover all the interatomic distances occurring in the data. For the loss function we have also added the root-mean-square (RMS) error of the forces to the DFT total energies, with a trade-off between energy and forces loss. The convergence is obtained when the loss function is less than  $10^{-4}$ . A  $\text{Mg}_n$  cluster test set of  $2 \times 10^5$  configurations ( $4 \times 10^5$  for  $\text{Mg}_n\text{H}_{2n}$ ) was used

for the determination of the Maximum Absolute Error (MAE) between ML predictions and the configurations of the test set.

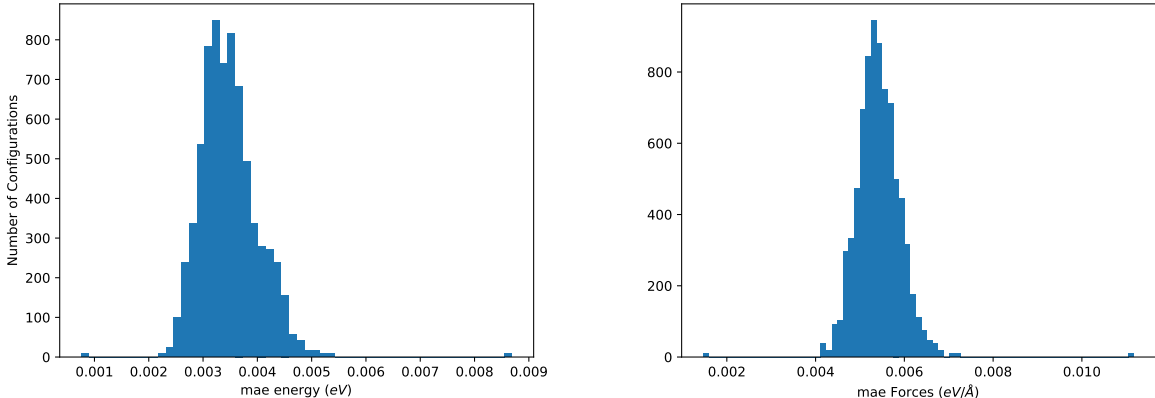


Figure 3: Left panel: MAE histogram distribution for the  $Mg_n$  test set of the DFT total energy and the relevant ML predictions. Right panel: MAE histogram distribution for the  $Mg_n$  test set of the DFT forces and the relevant ML predictions.

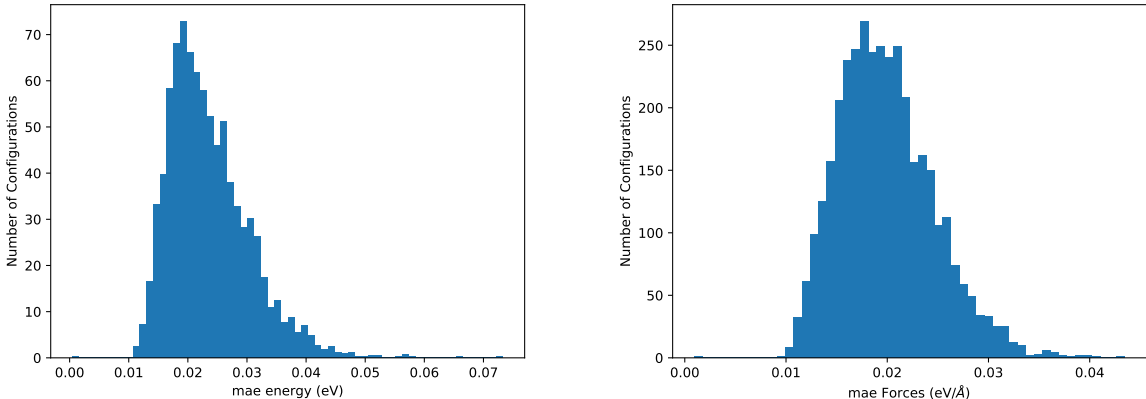


Figure 4: Left panel: MAE histogram distribution for the  $Mg_nH_{2n}$  test set of the DFT total energy and the relevant ML predictions. Right panel: MAE histogram distribution for the  $Mg_nH_{2n}$  test set of the DFT forces and the relevant ML predictions.

In Figs. (3)-(4), we report the MAE histogram distributions for the ML predictions and the test set configuration batches (the batch size is made by 128 geometrical configurations) for the case of  $Mg_n$  and  $Mg_nH_{2n}$ , respectively.

The MAE mean values for the  $Mg_n$  clusters are rather small, that is 0.004 eV for the energy and 0.005 eV/Å for the forces at the peak maximum (see Fig. (3)). The  $Mg_nH_{2n}$

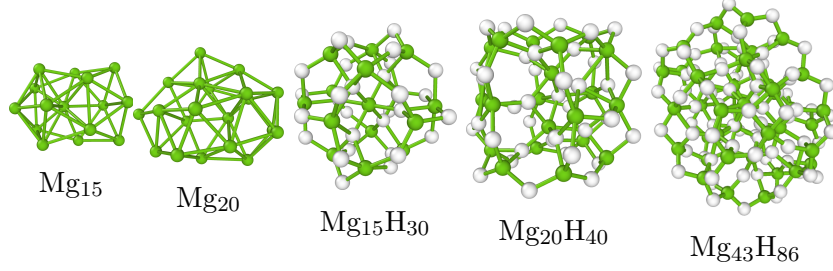


Figure 5: Mg and MgH<sub>2</sub> NPs structures optimized by using our S[chnet]SCHA approach with the inclusion of anharmonic corrections.

energies and forces are, respectively, 0.02 eV and 0.02 eV/Å around the maximum of the peak distributions (see Fig. (4)). The trained SchNet best model was embedded in the ASE calculator<sup>36</sup>, which provides the total energies and forces to be used in the SSCHA minimization procedure.

For  $n > 10$ , optimized Mg<sub>*n*</sub> and Mg<sub>*n*</sub>H<sub>2*n*</sub> geometries are reported in Figs. 5.

## Rotational entropy calculation of Mg and MgH<sub>2</sub> nanoclusters

Owing to the relatively high temperatures under investigation, we also assessed the contribution to the free energy of the rotational and vibrational degrees of freedom from statistical mechanics. The rotational entropy  $S_{rot}$  is expressed by<sup>48</sup>:

$$S_{rot} = k_B \ln \left[ \frac{\sqrt{\pi I_A I_B I_C}}{\sigma} \left( \frac{8\pi^2 k_B T}{h^2} \right)^{3/2} + \frac{3}{2} \right], \quad (8)$$

where  $I_A$ ,  $I_B$  and  $I_C$  are the three rotational principal moments of inertia corresponding to three mutually orthogonal directions, and  $h$  is the Planck constant. The symmetry number  $\sigma$  takes into account the entropy reduction by dividing by the number of pure rotational symmetries of the system. In our calculations, we used  $\sigma = 1$  which effectively sets an upper bound for the rotational entropy of the system.

## Calculation of the enthalpy and entropy of molecular hydrogen

The partition function of a gas of  $N$  identical and non-degenerate molecules is given by

$$Q(V, T) = \frac{1}{N!} \left( \frac{V}{\Lambda_M^3} q(T) \right)^N, \quad (9)$$

where  $q(T)$  is the partition function corresponding to the internal degrees of freedom and  $\Lambda_M = h/\sqrt{2\pi M k_B T}$ , is the de Broglie thermal wavelength associated with the molecule of mass  $M$ .

As discussed in the supplementary information the molecular partition function can be written as

$$q(T) = \sum'_L \sum_{n=1}^{N(L)} (2L+1) e^{-\beta E_{L,n}}, \quad (10)$$

where  $E_{L,n}$  are the energies of molecular eigenstates and the primed sum denotes the sum over the angular momenta relevant to identical or distinguishable isotopes.

From  $q(T)$ , one can calculate, respectively

i) the HFE as follows:

$$\begin{aligned} F &= -k_B T \ln(Q(V, T)) \\ &= N k_B T \log \left( \frac{P \Lambda_M^3}{k_B T} \right) - N k_B T - N k_B T \log(q(T)), \end{aligned} \quad (11)$$

ii) the average internal energy as:

$$\begin{aligned} U &= -\frac{\partial \ln(Q(V, T))}{\partial \beta} \\ &= \frac{3}{2} N k_B T + N \frac{\sum'_{L,n} (2L+1) E_{L,n} \exp^{-\beta E_{L,n}}}{\sum'_{L,n} (2L+1) e^{-\beta E_{L,n}}}, \end{aligned} \quad (12)$$

iii) and, finally, the entropy and the enthalpy of the H gas as:

$$S = \frac{U - F}{T}, \quad (13)$$

$$H = U + \frac{3Nk_{\text{B}}T}{2} + Nk_{\text{B}}T, \quad (14)$$

where the ideal gas law  $PV = Nk_{\text{B}}T$  has been used in the expression of  $F$  and  $H$ .

The calculation of Eq. (10) has been performed by diagonalizing the Hamiltonian  $\mathcal{H}$  in the subspace spanned by the states of angular momentum  $L$ . The vdW corrected pair potential  $V(R)$  is obtained from DFT simulations. We considered interatomic separations in the range  $0.2 - 2.5 \text{ \AA}$ , discretized in 1024 equally-spaced steps. We calculated  $\mathcal{H}$  in the basis of particles confined in a box of the same extension, limiting to the first 256 states.

The matrix diagonalization was carried out achieving an accuracy better than 1 part in  $10^4$  for temperatures less than  $5 \times 10^3 \text{ K}$ . We considered progressively higher angular momenta up to  $L_{\text{max}}$ , defined as the angular momentum whose ground-state energy is above  $5 \times 10^4 \text{ K}$  the minimum energy of the pair potential. Once the values  $E_{L,n}$  were obtained, the thermodynamic properties can be calculated using Eqs. (10) to (13).

## Results and Discussion

### Hydrogen thermodynamics

The calculations of entropy and enthalpy of H have been carried out according to Eqs. 4 and 5, respectively. We report the results in Tab. 1. The inclusion of the anharmonic correction to vibrations improves significantly the agreement with the experimental data<sup>49</sup>, as we obtain an error  $\leq 0.1\%$  with respect to previous estimates of  $\simeq 5\%$ <sup>3</sup>.

### Thermal expansion

Starting from known local minima structures at  $0 \text{ K}$ <sup>4,26,27</sup>, we optimized Mg and MgH<sub>2</sub> NPs at  $300 \text{ K}$  using the SSCHA method, where the centroid positions of the stochastic population correspond to the atomic positions (see Figs. 1 and 2 for Mg<sub>*n*</sub> and Mg<sub>*n*</sub>H<sub>2*n*</sub> NPs, respectively). In order to explore the influence of temperature on MgH<sub>2</sub> NPs we also computed the bond

Table 1: Bond lengths and thermodynamic properties of H<sub>2</sub>:  $S$ =entropy,  $H$ =enthalpy in comparison to experimental data (exp)<sup>49,50</sup>.

	This work (Å)	exp (Å) <sup>49</sup>
Bond length	0.746	0.741
	This work (meV/K)	exp (meV/K) <sup>50</sup>
$S_{(298.15K)}$	1.355	1.354
$S_{(500K)}$	1.511	1.510
$S_{(600K)}$	1.566	1.566
$H$	This work (meV)	exp (meV) <sup>49</sup>
$H_{(500K)}-H_{(298.15K)}$	0.0610	0.0609
$H_{(600K)}-H_{(500K)}$	0.0304	0.0304

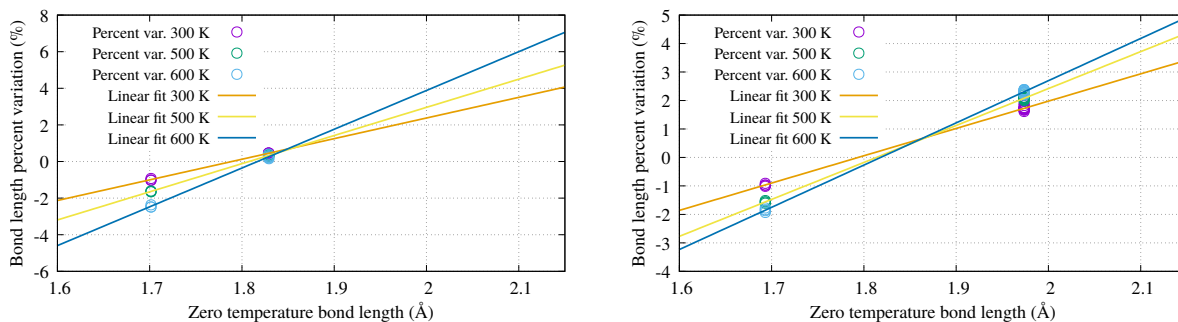


Figure 6: Percent variation of the Mg-H bond length with respect to their 0 K values (empty circles) in the temperature range 300-600 K for the Mg<sub>3</sub>H<sub>6</sub>-C (left panel) and Mg<sub>4</sub>H<sub>8</sub>-A (right panel) NPs. The Mg-H bond length increases with temperature for those bonds where H is multi-coordinated ( $\approx 1.98$  Å at 0 K), and decreases for single-coordinated H atoms ( $\approx 1.7$  Å at 0 K). The bond lengths of double-coordinated H atoms ( $\approx 1.83$  Å at 0 K) are unaffected by temperature.

lengths at 300 K, 500 K, and 600 K.

Furthermore, we reckon the percent variation of the Mg-H bond length with respect to their 0 K structures for all the MgH<sub>2</sub> NPs under investigation. In Fig. 6 we show the percent variation of the Mg-H bond length with respect to the 0 K value for Mg<sub>3</sub>H<sub>6</sub>-C (left panel) and of Mg<sub>4</sub>H<sub>8</sub>-A (right panel) NPs. These MgH<sub>2</sub> NPs clearly show that the Mg-H bond length increases with temperature for those bonds where H is multi-coordinated ( $\approx 1.98 \text{ \AA}$  at 0 K) and decreases for single-coordinated H atoms ( $\approx 1.7 \text{ \AA}$  at 0 K). The bond lengths for double-coordinated H atoms ( $\approx 1.83 \text{ \AA}$  at 0 K) are essentially unaffected by temperature. This picture can be extended to the other Mg<sub>n</sub>H<sub>2n</sub> NPs, and in the Supplementary Information (see Fig. 1S) we report similar plots for various Mg<sub>n</sub>H<sub>2n</sub> NPs in their local minima. The percent variation of the bond length due to temperature shows an approximately linear behaviour. In particular, by using a linear law to represent the percent variation  $g(l) = a(l - b)$ , where  $l$  is the 0 K bond length and  $a, b$  are fit parameters, we find that  $a$  is an increasing monotonic function of temperature, with values in the range  $6\text{-}11 \text{ \AA}^{-1}$ ,  $8\text{-}15 \text{ \AA}^{-1}$ , and  $9\text{-}21 \text{ \AA}^{-1}$ , for 300 K, 500 K, and 600 K, respectively. The parameter  $b$  is  $\simeq 1.7\text{-}1.8 \text{ \AA}$  with only a small increment from 300 K to 600 K.

## Thermodynamic properties

The thermodynamic properties per formula unit of several Mg and MgH<sub>2</sub> NPs at 300 K obtained from our SSCHA calculations are reported in Tabs. 2 and 3 (simulations were also carried out at 500 K and 600 K).

We notice that Mg<sub>n</sub> clusters present a free energy at 300 K always lower than the internal energy at 0 K ( $F(300) - U(0) < 0$ ), while the opposite trend was found for the Mg<sub>n</sub>H<sub>2n</sub> NPs. Although the result observed for Mg<sub>n</sub> does not allow to infer a significant contribution from anharmonicities (the negative sign of  $F(300) - U(0)$  is generally expected due to entropy increase even in harmonic systems), the destabilization of Mg<sub>n</sub>H<sub>2n</sub> NPs is a clear sign of the influence of anharmonicities.



Table 2: Thermodynamic properties of Mg NPs referred to Mg bulk formula unit at 0 K.  $U(0)$  = internal energy at 0 K,  $F(300)$  and  $S(300)$  are the free energy and entropy at 300 K, respectively.

Nanoparticle	$U(0)$ (meV)	$F(300)$ (meV)	$F(300) - U(0)$ (meV)	$S(300)$ (meV/K)
Mg <sub>3</sub> -A	1516	1494	-22	0.153
Mg <sub>4</sub> -A	1331	1321	-9	0.175
Mg <sub>5</sub> -A	1314	1285	-28	0.258
Mg <sub>6</sub> -A	1291	1252	-39	0.308
Mg <sub>7</sub> -A	1224	1191	-32	0.314
Mg <sub>8</sub> -A	1187	1155	-32	0.319
Mg <sub>9</sub> -A	1096	1074	-22	0.288
Mg <sub>10</sub> -A	1027	1006	-21	0.290

Furthermore, the free energy of Mg<sub>*n*</sub> clusters is a decreasing function of the NPs size. We also found that the entropy of Mg<sub>*n*</sub> nanoclusters shows an increasing trend up to  $n = 8$ , while presents a slight decrease above that value. The entropy of Mg<sub>*n*</sub>H<sub>2*n*</sub> NPs is in prevalence an increasing function of  $n$ . However, we notice that for a few small- $n$  Mg<sub>*n*</sub>H<sub>2*n*</sub> NPs the entropy exceeds that of large  $n$  ones.

## Hydrogen desorption temperature

The first-principles calculation of the desorption temperature  $T_d$ , which is of paramount importance to tailor the geometrical structure and the composition of the NPs to make them viable for hydrogen storage applications, was carried out by using Eq. (3). The dependence of  $T_d$  on the cluster size was reckoned using the lowest energy Mg<sub>*n*</sub> and Mg<sub>*n*</sub>H<sub>2*n*</sub> NPs for  $n \leq 10$ .

In this respect, we carried out three sets of calculations (shown in Fig. 7) using i) the harmonic approximation without rotational entropy (purple line); ii) the fully anharmonic SSCHA expression neglecting the contribution of the rotational entropy (green line); iii)

Table 3: Thermodynamic properties of  $\text{Mg}_n\text{H}_{2n}$  NPs referred to  $\text{MgH}_2$  bulk formula unit at 0 K.  $U(0)$ =internal energy at 0 K,  $F(300)$  and  $S(300)$  are the free energy and entropy at 300 K, respectively. (L) stands for lowest energy structure.

Nanoparticle	$U(0)$ (meV)	$F(300)$ (meV)	$F(300) - U(0)$ (meV)	$S(300)$ (meV/K)
$\text{Mg}_3\text{H}_6$ -A (L)	1645	1942	297	0.256
$\text{Mg}_3\text{H}_6$ -B	1667	1982	315	0.191
$\text{Mg}_3\text{H}_6$ -C	1733	2022	289	0.252
$\text{Mg}_4\text{H}_8$ -A	1507	1816	310	0.251
$\text{Mg}_4\text{H}_8$ -B	1537	1840	303	0.163
$\text{Mg}_4\text{H}_8$ -C	1562	1820	258	0.355
$\text{Mg}_4\text{H}_8$ -D	1416	1741	326	0.233
$\text{Mg}_4\text{H}_8$ -E	1511	1806	296	0.317
$\text{Mg}_4\text{H}_8$ -F (L)	1416	1741	326	0.237
$\text{Mg}_5\text{H}_{10}$ -A (L)	1300	1627	326	0.269
$\text{Mg}_5\text{H}_{10}$ -B	1311	1651	339	0.236
$\text{Mg}_6\text{H}_{12}$ -A	1246	1571	325	0.297
$\text{Mg}_6\text{H}_{12}$ -B (L)	1184	1513	326	0.295
$\text{Mg}_7\text{H}_{14}$ -A (L)	1094	1422	328	0.312
$\text{Mg}_7\text{H}_{14}$ -B	1119	1453	339	0.292
$\text{Mg}_8\text{H}_{16}$ -A (L)	995	1342	347	0.274
$\text{Mg}_8\text{H}_{16}$ -B	1024	1361	337	0.295
$\text{Mg}_9\text{H}_{18}$ -A (L)	967	1301	333	0.323
$\text{Mg}_{10}\text{H}_{20}$ -A (L)	883	1224	341	0.310

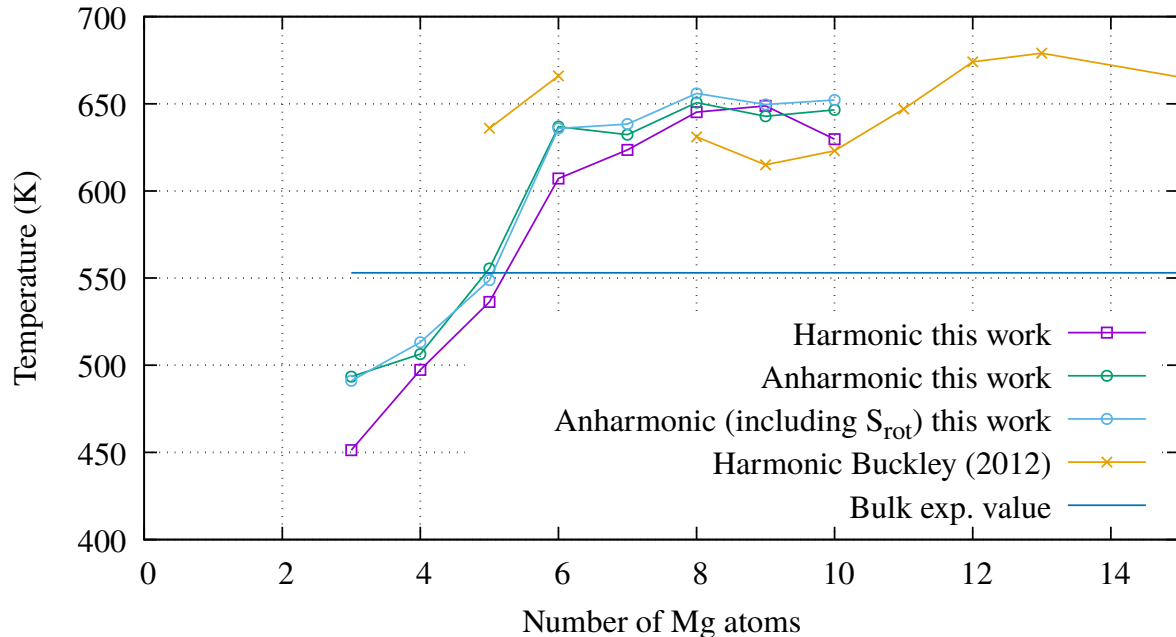


Figure 7: Desorption temperature of  $\text{MgH}_2$  NPs of increasing size, compared with the results obtained within the harmonic approximation<sup>3</sup>.

the fully anharmonic SSCHA expression including the rotational entropy (cyan line). In the latter case rotational and vibrational degrees of freedom were decoupled; the rotational entropy was computed including the thermal expansion of the atomic coordinates obtained from the SSCHA calculations. This reflects in the dependence of the rotational entropy (see Eq. 8) on both temperature and moments of inertia.

We report the results of these three calculations in Tab. 4 alongside with the desorption enthalpy and entropy for each case. Furthermore, we compare our results in Fig. 7 with those obtained within the harmonic approximation<sup>3</sup> and the bulk value. We notice that the general trend, common to all of the three approaches, points towards a destabilization of only the smaller NPs with respect to bulk. The increase of  $T_d$  with the number of atoms drives its value beyond the bulk desorption temperature. We also note that the difference between the harmonic approximation and the fully anharmonic calculation is small, although not negligible (up to 10%) but presents a remarkable dependence on the number of atoms.

Moreover, the inclusion of rotational entropy is essentially negligible and its contribution is almost independent of the NP size.

Table 4: Harmonic and anharmonic results for desorption temperature ( $T_d$ ), desorption enthalpy  $H(T_d)$  and desorption entropy  $S(T_d)$  of  $\text{MgH}_2$  NPs per unit formula at 0 K.

Reaction $\text{Mg}_n\text{H}_{2n} \rightarrow$ $\text{Mg}_n + (\text{H}_2)_n$	Harmonic			Anharmonic			Anharmonic including $S_{\text{rot}}$		
	$T_d$ (K)	$H(T_d)$ (meV)	$S(T_d)$ (meV/K)	$T_d$ (K)	$H(T_d)$ (meV)	$S(T_d)$ (meV/K)	$T_d$ (K)	$H(T_d)$ (meV)	$S(T_d)$ (meV/K)
$n = 3$	451	607	1.35	493	635	1.29	491	635	1.29
$n = 4$	497	670	1.35	506	684	1.35	513	684	1.33
$n = 5$	536	766	1.43	555	775	1.39	549	775	1.41
$n = 6$	607	851	1.40	637	875	1.44	636	876	1.44
$n = 7$	623	874	1.40	632	885	1.40	638	887	1.39
$n = 8$	645	936	1.45	651	958	1.47	656	952	1.45
$n = 9$	649	871	1.34	643	887	1.38	649	884	1.36
$n = 10$	630	888	1.41	646	897	1.39	652	895	1.37

Finally, our results for  $T_d$  are in good agreement with those obtained in Ref.<sup>3</sup> for  $n > 8$ , while for smaller nanoclusters they deviate significantly. We observe a systematic difference at an intermediate number of atoms; we attribute it to the fact that different local minima have been used in our case. In our procedure, indeed, we start by known local minima of amorphous structures and we include the effect of finite temperatures via SSCHA, while in Ref.<sup>3</sup> the NPs are trimmed from crystalline phase and further optimized. A main consequence of our approach is that our desorption temperature as a function of  $n$  (see Fig. 7) has a smoother behavior around  $n = 7$  than that found in Ref.<sup>3</sup>.

## Application of S[chnet]SCHA to larger nanoparticles

To compute the thermodynamic properties of NPs with  $n > 10$  as typically found in experiments, we applied our S[chnet]SCHA approach to a set of  $\text{Mg}_n$  ( $n = 15, 20$ ) and  $\text{Mg}_n\text{H}_{2n}$  ( $n = 15, 20$ ) NPs (see the optimized configurations in Fig. 5). The geometries were initially

Table 5: Comparison between the thermodynamic properties of the  $\text{Mg}_{10}$  and  $\text{Mg}_{10}\text{H}_{20}$  NPs computed by ab initio (AI) and our S[chnet]SCHA (ML) approaches, respectively. Thermodynamic properties refer to  $\text{MgH}_2$  bulk formula unit at 0 K.  $U(0)$  = internal energy at 0 K,  $F(300)$  and  $S(300)$  are the free energy and entropy at 300 K, respectively;  $T_d$ = desorption temperature.

Nanoparticle	$U(0)$ (meV)	$F(300)$ (meV)	$F(300) - U(0)$ (meV)	$S(300)$ (meV/K)	$T_d$ (K)
$\text{Mg}_{10}$ -A (AI)	1027	1006	-21	0.290	
$\text{Mg}_{10}$ -A (ML)	1027	1006	-20	0.289	
$\text{Mg}_{10}\text{H}_{20}$ (AI)	883	1226	343	0.308	646
$\text{Mg}_{10}\text{H}_{20}$ (ML)	883	1224	341	0.310	645

optimized by using a BFGS minimization algorithm<sup>36</sup> with the artificial neural network potentials. Minor changes in the atomic coordinates were found with respect to the starting configurations of the similar  $\text{Ti}_n\text{O}_{2n}$  NPs. The dynamical matrices for these input configurations were computed using ASE<sup>36</sup>. In Tab. 5 we compare the thermodynamic properties of the  $\text{Mg}_{10}$  and  $\text{Mg}_{10}\text{H}_{20}$  NPs computed by ab initio (AI) and our S[chnet]SCHA (ML) approaches, including the desorption temperature. We notice that the agreement is remarkable, thus validating our ML method.

Furthermore, in Tab. 6 we report the thermodynamic properties at 300 K for  $\text{Mg}_n\text{H}_{2n}$  ( $n = 15, 20$ ), that would have been very demanding with DFT-computed energies and forces. While these calculations refer to a local minimum, they only aim to show the applicability of our S[chnet]SCHA approach to carry out computational effective minimization of the free energy of these large NPs, running on a laptop.

## Conclusions

In this work we analyse the effect of anharmonicity in the interatomic potential on finite temperature properties, such as the free energy and entropy, for Mg and  $\text{MgH}_2$  NPs using the SSCHA approach. In particular, we use ab initio simulations to find the NPs optimized

geometries by relaxation of the stochastic populations centroids, corresponding to the average atomic positions. We also investigate the thermal expansion of Mg and MgH<sub>2</sub> NPs, finding a relative Mg-H bond length increase proportional to the 0 K value and a decrease in the Mg-H bond length when H is single-coordinated. In general, the contribution of anharmonicity is small for small size NPs.

Table 6: Thermodynamic properties of Mg and Mg<sub>n</sub>H<sub>2n</sub> NPs with  $n > 10$ , per formula unit, using our S[chnet]SCHA approach. Thermodynamic properties refer to MgH<sub>2</sub> bulk formula unit at 0 K.  $U(0)$  = internal energy at 0 K,  $F(300)$  and  $S(300)$  are the free energy and entropy at 300 K, respectively.

Nanoparticle	$U(0)$ (meV)	$F(300)$ (meV)	$F(300) - U(0)$ (meV)	$S(300)$ (meV/K)
Mg <sub>15</sub>	956	983	27	0.236
Mg <sub>20</sub>	883	996	113	0.354
Mg <sub>15</sub> H <sub>30</sub>	797	1187	389	0.341
Mg <sub>20</sub> H <sub>40</sub>	721	1132	411	0.383

Moreover, we compute from ab initio simulations the H<sub>2</sub>  $T_d$  in Mg<sub>n</sub>H<sub>2n</sub> NPs ( $n < 10$ ), including such anharmonicity. We find that i)  $T_d$  is an increasing function of the cluster size for the considered NPs; ii) the effect of anharmonicity on  $T_d$  is relatively small for small clusters (such as Mg<sub>3</sub>H<sub>6</sub>) while is more significant ( $\simeq 40$  K) for larger ones (such as Mg<sub>6</sub>H<sub>12</sub>). The inclusion of the rotational entropy in the calculation of desorption temperature leads to almost negligible corrections.

To extend the application of the SSCHA method to large Mg-based NPs we used the computationally expensive DFT calculations performed on several small clusters with similar bonding schemes for training a neural network to determine the forces and total energies of large nanoclusters. In particular, we adopted a Machine Learning approach based on the SchNet Neural-Network package, integrating the latter with the Atomic Simulation Environment and the Stochastic Self Consistent Harmonic Approximation python code. We applied our S[chnet]SCHA algorithm to the calculation of thermodynamic properties of Mg<sub>n</sub>H<sub>2n</sub> NPs up to  $n = 43$ , significantly increasing the size of NPs at a very small computational cost with

respect to ab initio simulations while keeping their accuracy. Indeed, the results we obtained using ab initio or ML approaches are in good agreement with respect to both thermodynamic properties and desorption temperature. This proof of concept demonstrates the viability of using ML-based methods to study the H desorption characteristics in magnesium clusters with realistic size.

Finally, our method can be adopted as high throughput screening of the thermodynamic properties and free-energy landscape exploration of large NPs, possibly relying for the training on hybrid functional DFT calculations<sup>25</sup>.

## Acknowledgement

The authors acknowledge Bruno Kessler Foundation (FBK) for providing unlimited access to the KORE computing facility. P.E.T. acknowledges the Q@TN consortium for his support. This work was partially realized with the financial support of Caritro Foundation (Cassa di Risparmio di Trento e Rovereto, Italy) by the project “*High-Z ceramic oxide nanosystems for mediated proton cancer therapy*”. The research is also partially funded by the Ministry of Science and Higher Education of the Russian Federation as part of World-class Research Center program: Advanced Digital Technologies (contract No. 075-15-2020-934 dated 17.11.2020). Finally, the authors acknowledge fruitful discussions with I. Errea, M. Calandra and F. Mauri, who also kindly provided the beta-version of the SSCHA code.

## Supporting Information Available

Further theoretical and computational procedures, convergence tests and characterization data for all new compounds.

## References

- (1) Chen, Y.-L.; Huang, C.-H.; Hu, W.-P. Theoretical Study on the Small Clusters of LiH, NaH, BeH<sub>2</sub>, and MgH<sub>2</sub>. *The Journal of Physical Chemistry A* **2005**, *109*, 9627–9636, PMID: 16866416.
- (2) Wu, Z.; Allendorf, M. D.; Grossman, J. C. Quantum Monte Carlo Simulation of Nanoscale MgH<sub>2</sub> Cluster Thermodynamics. *Journal of the American Chemical Society* **2009**, *131*, 13918–13919.
- (3) Buckley, A. C.; Carter, D. J.; Sheppard, D. A.; Buckley, C. E. Density Functional Theory Calculations of Magnesium Hydride: A Comparison of Bulk and Nanoparticle Thermodynamics. *The Journal of Physical Chemistry C* **2012**, *116*, 17985–17990.
- (4) Shevlin, S. A.; Guo, Z. X. MgH<sub>2</sub> Dehydrogenation Thermodynamics: Nanostructuring and Transition Metal Doping. *The Journal of Physical Chemistry C* **2013**, *117*, 10883–10891.
- (5) Hussain, T.; Maark, T. A.; Chakraborty, S.; Ahuja, R. Improvement in Hydrogen Desorption from  $\beta$ - and  $\gamma$ -MgH<sub>2</sub> upon Transition-Metal Doping. *ChemPhysChem* **2015**, *16*, 2557–2561.
- (6) Shen, C.; Aguey-Zinsou, K.-F. Can  $\gamma$ -MgH<sub>2</sub> improve the hydrogen storage properties of magnesium? *Journal of Materials Chemistry A* **2017**, *5*, 8644–8652.
- (7) Kumar, E. M.; Rajkamal, A.; Thapa, R. Screening based approach and dehydrogenation kinetics for MgH<sub>2</sub>: Guide to find suitable dopant using first-principles approach. *Scientific Reports* **2017**, *7*.
- (8) Zhang, J.; Xia, G.; Guo, Z.; Zhou, D. Synergetic Effects toward Catalysis and Confinement of Magnesium Hydride on Modified Graphene: A First-Principles Study. *The Journal of Physical Chemistry C* **2017**, *121*, 18401–18411.



- (9) Pasquini, L. The Effects of Nanostructure on the Hydrogen Sorption Properties of Magnesium-Based Metallic Compounds: A Review. *Crystals* **2018**, *8*, 106.
- (10) Yartys, V. et al. Magnesium based materials for hydrogen based energy storage: Past, present and future. *International Journal of Hydrogen Energy* **2019**, *44*, 7809–7859.
- (11) Battisti, A.; Taioli, S.; Garberoglio, G. Zeolitic imidazolate frameworks for separation of binary mixtures of CO<sub>2</sub>, CH<sub>4</sub>, N<sub>2</sub> and H<sub>2</sub>: A computer simulation investigation. *Microporous and Mesoporous Materials* **2011**, *143*, 46–53.
- (12) Garberoglio, G.; Pugno, N.; Taioli, S.; Simone, Gas Adsorption and Separation in Realistic and Idealized Frameworks of Organic Pillared Graphene: A Comparative Study. *The Journal of Physical Chemistry C* **2014**, *119*, 1980–1987.
- (13) Garberoglio, G.; Taioli, S. Modeling flexibility in metal–organic frameworks: comparison between density-functional tight-binding and universal force field approaches for bonded interactions. *Microporous and mesoporous materials* **2012**, *163*, 215–220.
- (14) Pedrielli, A.; Taioli, S.; Garberoglio, G.; Pugno, N. M. Gas adsorption and dynamics in Pillared Graphene Frameworks. *Microporous and Mesoporous Materials* **2018**, *257*, 222–231.
- (15) Schlapbach, L.; Züttel, A. Hydrogen-storage materials for mobile applications. *Nature* **2001**, *414*, 353–358.
- (16) Sakintuna, B.; Lamardarkrim, F.; Hirscher, M. Metal hydride materials for solid hydrogen storage: A review. *International Journal of Hydrogen Energy* **2007**, *32*, 1121–1140.
- (17) Webb, C. A review of catalyst-enhanced magnesium hydride as a hydrogen storage material. *Journal of Physics and Chemistry of Solids* **2015**, *84*, 96–106.
- (18) Hanada, N.; Ichikawa, T.; Fujii, H. Hydrogen absorption kinetics of the catalyzed MgH<sub>2</sub> by niobium oxide. *Journal of Alloys and Compounds* **2007**, *446-447*, 67 – 71, Proceed-

ings of the International Symposium on Metal-Hydrogen Systems, Fundamentals and Applications (MH2006).

- (19) He, D.; Wang, Y.; Wu, C.; Li, Q.; Ding, W.; Sun, C. Enhanced hydrogen desorption properties of magnesium hydride by coupling non-metal doping and nano-confinement. *Applied Physics Letters* **2015**, *107*, 243907.
- (20) Varin, R. A.; Czujko, T.; Wronski, Z. Particle size, grain size and  $\gamma$ -MgH<sub>2</sub> effects on the desorption properties of nanocrystalline commercial magnesium hydride processed by controlled mechanical milling. *Nanotechnology* **2006**, *17*, 3856–3865.
- (21) Aguey-Zinsou, K.-F.; Ares-Fernández, J.-R. Synthesis of Colloidal Magnesium: A Near Room Temperature Store for Hydrogen. *Chemistry of Materials* **2008**, *20*, 376–378.
- (22) Paskevicius, M.; Sheppard, D. A.; Buckley, C. E. Thermodynamic Changes in Mechanochemically Synthesized Magnesium Hydride Nanoparticles. *Journal of the American Chemical Society* **2010**, *132*, 5077–5083.
- (23) Wagemans, R. W. P.; van Lenthe, J. H.; de Jongh, P. E.; van Dillen, A. J.; de Jong, K. P. Hydrogen Storage in Magnesium Clusters: Quantum Chemical Study. *Journal of the American Chemical Society* **2005**, *127*, 16675–16680.
- (24) Kim, K. C.; Dai, B.; Johnson, J. K.; Sholl, D. S. Assessing nanoparticle size effects on metal hydride thermodynamics using the Wulff construction. *Nanotechnology* **2009**, *20*, 204001.
- (25) Koukaras, E. N.; Zdetsis, A. D.; Sigalas, M. M. Ab Initio Study of Magnesium and Magnesium Hydride Nanoclusters and Nanocrystals: Examining Optimal Structures and Compositions for Efficient Hydrogen Storage. *Journal of the American Chemical Society* **2012**, *134*, 15914–15922.

- (26) Belyaev, S. N.; Panteleev, S. V.; Ignatov, S. K.; Razuvaev, A. G. Structural, electronic, thermodynamic and spectral properties of  $Mg_n$  ( $n=2-31$ ) clusters. A DFT study. *Computational and Theoretical Chemistry* **2016**, *1079*, 34–46.
- (27) Duanmu, K.; Roberto-Neto, O.; Machado, F. B. C.; Hansen, J. A.; Shen, J.; Piecuch, P.; Truhlar, D. G. Geometries, Binding Energies, Ionization Potentials, and Electron Affinities of Metal Clusters:  $Mg_n^{0,\pm 1}$ ,  $n = 1-7$ . *The Journal of Physical Chemistry C* **2016**, *120*, 13275–13286.
- (28) Cui, J.; Ouyang, L.; Wang, H.; Yao, X.; Zhu, M. On the hydrogen desorption entropy change of modified  $MgH_2$ . *Journal of Alloys and Compounds* **2018**, *737*, 427–432.
- (29) San-Martin, A.; Manchester, F. D. The H-Mg (Hydrogen-Magnesium) system. *Journal of Phase Equilibria* **1987**, *8*, 431–437.
- (30) Bastide, J.-P.; Bonnetot, B.; Lètoffè, J.-M.; Claudy, P. Polymorphisme de l'hydrure de magnésium sous haute pression. *Materials Research Bulletin* **1980**, *15*, 1779–1787.
- (31) Errea, I.; Calandra, M.; Mauri, F. Anharmonic free energies and phonon dispersions from the stochastic self-consistent harmonic approximation: Application to platinum and palladium hydrides. *Physical Review B* **2014**, *89*.
- (32) Bianco, R.; Errea, I.; Paulatto, L.; Calandra, M.; Mauri, F. Second-order structural phase transitions, free energy curvature, and temperature-dependent anharmonic phonons in the self-consistent harmonic approximation: Theory and stochastic implementation. *Phys. Rev. B* **2017**, *96*, 014111.
- (33) Monacelli, L.; Errea, I.; Calandra, M.; Mauri, F. Pressure and stress tensor of complex anharmonic crystals within the stochastic self-consistent harmonic approximation. *Physical Review B* **2018**, *98*.

- (34) Grimme, S.; Antony, J.; Ehrlich, S.; Krieg, H. A consistent and accurate ab initio parametrization of density functional dispersion correction (DFT-D) for the 94 elements H-Pu. *The Journal of Chemical Physics* **2010**, *132*, 154104.
- (35) Schütt, K. T.; Saucedo, H. E.; Kindermans, P.-J.; Tkatchenko, A.; Müller, K.-R. SchNet - A deep learning architecture for molecules and materials. *The Journal of Chemical Physics* **2018**, *148*, 241722.
- (36) Larsen, A. H.; et al, The atomic simulation environment: a Python library for working with atoms. *Journal of Physics: Condensed Matter* **2017**, *29*, 273002.
- (37) Monacelli, L.; Bianco, R.; Cherubini, M.; Calandra, M.; Errea, I.; Mauri, F. The stochastic self-consistent harmonic approximation: Calculating vibrational properties of materials with full quantum and anharmonic effects. *Journal of Physics: Condensed Matter* **2021**, *33*.
- (38) Huang, K. *Statistical Mechanics*; John Wiley & Sons, 1987.
- (39) Giannozzi, P. et al. Advanced capabilities for materials modelling with Quantum ESPRESSO. *Journal of Physics: Condensed Matter* **2017**, *29*, 465901.
- (40) Perdew, J. P.; Burke, K.; Ernzerhof, M. Generalized Gradient Approximation Made Simple. *Phys. Rev. Lett.* **1996**, *77*, 3865–3868.
- (41) Grimme, S. Semiempirical GGA-type density functional constructed with a long-range dispersion correction. *Journal of Computational Chemistry* **2006**, *27*, 1787–1799.
- (42) Makov, G.; Payne, M. C. Periodic boundary conditions in ab initio calculations. *Physical Review B* **1995**, *51*, 4014–4022.
- (43) Martyna, G. J.; Tuckerman, M. E. A reciprocal space based method for treating long range interactions in ab initio and force-field-based calculations in clusters. *The Journal of Chemical Physics* **1999**, *110*, 2810–2821.

- (44) Hernández, A. B.; Hernández, W. I.; Cid, A. P.; García, J. C.; Villanueva, M. S. Prediction, and physic-chemical properties of (TiO<sub>2</sub>)<sub>n=15–20</sub> clusters and their possible catalytic application: A DFT study. *Computational Materials Science* **2019**, *162*, 228–235.
- (45) Lamiel-Garcia, O.; Cuko, A.; Calatayud, M.; Illas, F.; Bromley, S. T. Predicting size-dependent emergence of crystallinity in nanomaterials: titania nanoclusters versus nanocrystals. *Nanoscale* **2017**, *9*, 1049–1058.
- (46) Morales-García, Á.; Escatllar, A. M.; Illas, F.; Bromley, S. T. Understanding the interplay between size, morphology and energy gap in photoactive TiO<sub>2</sub> nanoparticles. *Nanoscale* **2019**, *11*, 9032–9041.
- (47) Shen, D.; Kong, C.-P.; Jia, R.; Fu, P.; Zhang, H.-X. Investigation of Properties of Mgn Clusters and Their Hydrogen Storage Mechanism: A Study Based on DFT and a Global Minimum Optimization Method. *The Journal of Physical Chemistry A* **2015**, *119*, 3636–3643.
- (48) Moore, W. J. *Physical Chemistry*; London: Longmans Green, 1963.
- (49) Chase, J., M. W. NIST-JANAF Thermochemical Tables. *J. Phys. Chem. Ref. Data*, *4th ed.* American Institute of Physics: New York **1998**,
- (50) Herzberg, G.; Howe, L. L. The Lyman bands of Molecular Hydrogen. *Canadian Journal of Physics* **1959**, *37*, 636–659.